# A Wavelet Phase Filter for Emission Tomography

Elwood T. Olsen and Biquan Lin*

Department of Mathematics
Illinois Institute of Technology
Chicago, IL 60616
E-mail: vefolsen@minna.iit.edu, blin@mcs.anl.gov

**Abstract**

The presence of a high level of noise is a characteristic in some tomographic imaging techniques such as positron emission tomography (PET). Wavelet methods can smooth out noise while preserving significant features of images. Mallat et al. proposed a wavelet based denoising scheme exploiting wavelet modulus maxima, but the scheme is sensitive to noise. In this study, we explore the properties of *wavelet phase*, with a focus on reconstruction of emission tomography images. Specifically, we show that the wavelet phase of regular Poisson noise under a Haar-type wavelet transform converges in distribution to a random variable uniformly distributed on $[0, 2\pi)$. We then propose three wavelet-phase-based denoising schemes which exploit this property: edge tracking, local phase variance thresholding, and scale phase variation thresholding. Some numerical results are also presented. The numerical experiments indicate that wavelet phase techniques show promise for wavelet based denoising methods.

Keywords: Wavelet phase, image reconstruction, denoising, Haar transform

## 1 Introduction

In positron emission tomography (PET), some image reconstruction technique is needed to process measurements of observed photons (the "sinogram data") into an easily grasped visual image. Image reconstruction algorithms currently in use are based on Fourier transform techniques. The convolution back projection method (CBP) and direct Fourier reconstruction method (DFR), [STAR81], are the most commonly used image reconstruction methods. These algorithms are, however, sensitive to noise in the measurements. In particular, noise is a problem in emission tomography. In PET applications, the sinogram data is an image which may have an average

*Currently in the Mathematics and Computer Science Division of Argonne National Laboratory, supported by the Office of Scientific Computing, U.S. Department of Energy, under Contract W-31-109-Eng-38.

## DISCLAIMER

Portions of this document may be illegible in electronic image products. Images are produced from the best available original document.

photon density of order 10 photons per pixel (nearer 100 per pixel in the numerical experiments described here) and hence is inherently noisy.

One way to reduce noise sensitivity is to model the emission process as a random process and to use reconstruction algorithms based on the statistical model. In 1982, Shepp and Vardi [SHEP82] introduced a Poisson process model for emission tomography which seems to be an excellent model. Maximum likelihood (ML) and maximum a posteriori (MAP) methods based on this model give what we consider to be the best possible reconstruction from noisy sinogram data.

The problem with the ML and MAP techniques is that they are very expensive in comparison with Fourier based techniques. The DFR method requires $O(N^2 \log N)$ operations, and CBP requires $O(N^3)$ operations, where $N$ is the number of detectors. On the other hand, an iterative ML algorithm (called the EM algorithm) requires $O(N^4)$ operations for each iteration and it usually takes 50 iterations to achieve sufficient precision, [VARD85]. Even with acceleration techniques such as Lewitt and Muehllehner's relaxation method, [LEWI86], the EM algorithm still remains computationally very expensive.

Another way to reduce noise sensitivity is to filter the sinogram data. Several filtering techniques for emission tomography are described in the literature. Linear low pass filters are easy to implement in connection with Fourier based methods, and are the current method of choice. A special lowpass filter called the parabola filter was developed at Washington University for the purpose of PET noise reduction. The filter is called a "parabola" filter since the window function is a quadratic function in the frequency domain (the filter is nonetheless a linear filter). The window function is the product of a triangle function

$$u(\omega) = \frac{\omega}{\Omega}\delta_{[-\Omega,\Omega]}(\omega)$$

and a ramp function

$$u(\omega) = \frac{\Omega - \omega}{\Omega}\delta_{[-\Omega,\Omega]}(\omega)$$

where $\Omega$ is the cutoff frequency. Yang, [YANG91], implemented a noise filtering scheme using projection onto convex sets. Kuan et al., [KUAN85], developed an adaptive filter for PET image restoration. According to Yang's simulation results, the parabola filter is among the most effective for use in connection with the CBP method, from the standpoint of subjective evaluation of the resulting reconstructed image. The underlying assumption for using a lowpass filter such as the parabola filter is that the energy of a typical image is primarily concentrated in its low-frequency components and that the energy of a random noise is more spread out over the whole frequency domain. While this assumption seems to be a reasonable one even for the noise in emission tomography, it is not clear to us that this assumption alone captures the significant features of the noise present in emission tomography applications. In these applications, the noise is signal-dependent Poisson type noise. Furthermore, while the gross structure of an image appears as low-frequency components, sharp edges give rise to high-frequency components, and small details also give rise to high-frequency components. Therefore, the linear lowpass filtering

unavoidably causes some blurring of edges and loss of detail from the original image. This can be a serious problem in medical imaging applications, where details may contain the most important messages in the image.

Conventional linear filtering schemes investigated so far are not very satisfactory. The motivation of the research described here was to design an effective and inexpensive filter which took into account the signal dependent Poisson noise occurring in emission tomography. We wanted to obtain an improved but still inexpensive filtering technique which could provide image quality from inexpensive Fourier methods comparable to that achievable with expensive ML type methods.

The filter we have developed is based on a wavelet technique. Basically, edges in a wavelet transform of the sinogram data at several scales are obtained using a magnitude (or modulus maximum) method, spurious edges are discarded using wavelet "phase" information, and a filtered or restored sinogram is obtained from retained (hopefully, "true") edges at various scales. The CBP or DFR method is then used to reconstruct the image from the restored sinogram.

Signal restoration techniques based on wavelets are often designed and tested using one-dimensional signals, then applied to two-dimensional signals (images). Mallat et al. [MALL92 a, b] proposed a multiscale edge detection and reconstruction scheme which makes use of modulus maxima of wavelet transforms. Our technique is based on that of Mallat et al., but it makes use of the "phase," or direction, of the two-dimensional wavelet transform as well as the magnitude of its modulus. The phase is a characteristic of two-dimensional wavelets without a one-dimensional counterpart. Numerical experiments indicate that wavelet phase methods show promise for denoising in emission tomography applications.

The remainder of this paper is organized as follows: Section II introduces wavelet based denoising methods, including wavelet phase based filtering schemes proposed here. Section III describes numerical experiments and discusses results.

# 2 Wavelet Based Denoising

In this section, we summarize wavelet modulus maxima based image representation and restoration methods proposed by Mallat and Zhong [MALL92a], Mallat and Hwang [MALL92b], and we introduce wavelet phase based methods.

**Wavelet Modulus and Phase.** Let $f$ denote a discrete image; $g$, a lowpass filter; $h_x$, a highpass filter in the $x$ direction; and $h_y$, a highpass filter in the $y$ direction. Let

$$g^0 = 1 \tag{1}$$

$$g^j = g^{j-1} \star g, \; j > 0 \tag{2}$$

where $\star$ denotes a linear convolution. The wavelet transform of the image $f$ at scale $j$ is defined by

$$(W_x^j f, W_y^j f, S^j f) = (h_x \star (g^{j-1} \star f), h_y \star (g^{j-1} \star f), g^j \star f). \tag{3}$$

The original image $f = S^0 f$ can be reconstructed by an inverse wavelet transform:

$$S^{j-1} f = h_x^* \star W_x^j f + h_y^* \star W_y^j f + g^* \star S^j f \tag{4}$$

where $h_x^*$, $h_y^*$ and $g^*$ satisfy

$$h_x^* \star h_x(m,n) + h_y^* \star h_y(m,n) + g^* \star g(m,n) = \delta(m,n) \tag{5}$$

where $\delta(m,n)$ is equal to 1 if m=n=0 and equal to 0 otherwise.

In our study, the filters $g$, $h_x$ and $h_y$ are those of the 2D symmetric Haar transform:

$$h_x = \frac{1}{4}\begin{bmatrix} 1 & 0 & -1 \\ 0 & 0 & 0 \\ 1 & 0 & -1 \end{bmatrix}, \tag{6}$$

$$h_y = \frac{1}{4}\begin{bmatrix} -1 & 0 & -1 \\ 0 & 0 & 0 \\ 1 & 0 & 1 \end{bmatrix} \tag{7}$$

and

$$g = \frac{1}{8}\begin{bmatrix} 1 & 0 & 0 & 0 & 1 \\ 0 & 0 & 0 & 0 & 0 \\ 0 & 0 & 4 & 0 & 0 \\ 0 & 0 & 0 & 0 & 0 \\ 1 & 0 & 0 & 0 & 1 \end{bmatrix}. \tag{8}$$

Let $h_x^* = -h_x$, $h_y^* = -h_y$ and $g^*(i,j) = \delta(i,j)$. Then, $h_x$, $h_y$, $g$, $h_x^*$, $h_y^*$ and $g^*$ satisfy (5) so that the original image can be reconstructed by inverse wavelet transform (4).

The wavelet modulus of $f$ at scale $j$ is defined by

$$M^j f = \sqrt{(W_x^j f)^2 + (W_y^j f)^2} \tag{9}$$

and the wavelet phase of $f$ at scale $j$ is defined by

$$P^j f = \text{Arctan}\frac{W_y^j f}{W_x^j f} \tag{10}$$

$$= \begin{cases} \arctan \frac{W_y^j f}{W_x^j f} & W_x^j f \geq 0, W_y^j f \geq 0 \\ \arctan \frac{W_y^j f}{W_x^j f} + \pi & W_x^j f < 0 \\ \arctan \frac{W_y^j f}{W_x^j f} + 2\pi & W_x^j f \geq 0, W_y^j f < 0 \end{cases} \tag{11}$$

The wavelet transform $(W_x^j f, W_y^j f)$ at scale $j$ is the gradient of some smoothed version of the image $f$ (though not in general the smoothed version of the image obtained by forming the convolution $f \star g^j$). Edges in the smoothed version of a signal are identified with curves along which the modulus of the gradient is large. The local tangent to an edge curve can be expected to be perpendicular to the gradient direction and to vary in a smooth manner from pixel to pixel along the edge, if the edge is a true edge and not an artifact of noise. This expected correlation in the phase of the wavelet transform at neighboring modulus maxima locations, together with the complementary fact, discussed below, that the wavelet phase associated with noise can be expected to be nearly uniformly distributed on the interval $[0, 2\pi)$, is the key fact which the wavelet phase based methods proposed here are designed to exploit.

**Wavelet Modulus Maxima Method.** In the early 80's, Marr and Hildreth [MARR80] introduced multiscale edge detection method. They provided a scheme which filters the original image via a series of low-pass filters with different cutoff frequencies (scales) and detects edges for each filtered image. In their approach, a Gaussian-type lowpass filter is used as the lowpass filter and the Laplacian method is used to find edge locations in the filtered images. Mallat and Zhong [MALL92a] refined Marr and Hildreth's approach in the setting of wavelets. In their technique, the wavelet transform of a noisy image is obtained, and all components of the wavelet transform except those corresponding to modulus maxima are discarded (in effect, set to zero). Since noise gives rise to spurious modulus maxima in the wavelet transform, only those modulus maxima above a certain threshold value are retained; alternatively, since modulus maxima due to noise are expected to decay more rapidly from scale to scale then modulus maxima due to true edges, the only those modulus maxima which exhibit the correct decay rate from scale to scale are retained; thus, some modulus maxima are attributed to noise and are discarded, or set to zero, along with the wavelet transform components at non-modulus-maximum locations. The method of Mallat et al., unlike that of Marr and Hildreth, is associated with a natural technique for reconstructing the image from the edge data. The discarded components of the wavelet transform are replaced via interpolation from the retained components, the "true" modulus maxima of the wavelet transform, and an inverse wavelet transform is then performed. The algorithm is summarized as follows:

1. Take discrete wavelet transforms of the contaminated image.
2. Obtain edge locations by finding local modulus maxima of wavelet transforms.
3. Remove those edges whose moduli either are below a given threshold or else decay faster than some given ratio or both.
4. Restore discarded wavelet transform components using an interpolation scheme.
5. Reconstruct signal from the restored wavelet transform by taking the inverse wavelet transform.

Numerical experiments indicate that the algorithm behaves well, at least in applications where the noise level is relatively low.

**Limitations of the Modulus based Approach.** The wavelet modulus maximum based method does not perform well in the medical imaging application considered here. The basic reason seems to be that a magnitude based scheme is sensitive to the magnitude of the noise, or more precisely, to the magnitude the variance of the noise. To remove noise of a large variance, the thresholds below which modulus maxima are discarded must be large. Since the noise in emission tomography applications has relatively large variance, the resulting large thresholds lead to discarding a lot of information about true edges. In addition, although it is shown in [MALL92b] that the wavelet modulus maxima of noise decay faster than modulus maxima of true signals from scale to scale under some circumstances, we have not observed a substantial difference in the decay rates in the application considered here. See [LIN94] for details.

**Wavelet Phase Filter Method.** As noted above the modulus maxima based method does not take into account the expected correlation between phase of the wavelet transform between neighboring edge pixels of an image. In [MALL92b], it was mentioned that one might incorporate wavelet phase information into their basic approach. We have tried to do this, and we describe the analysis and the resulting methods here.

The distribution of wavelet phase of noise can be characterized, if one assumes the statistical model which Shepp and Vardi developed. We state results here and refer the reader to [LIN94] for proofs of the next two theorems.

Let **L**={(i,j): i,j are integers} be a two-dimensional lattice. A stochastically modeled discrete image is a collection of random variables indexed in the lattice **L**, denoted by {X(i,j): (i,j) $\in$ **L**}. (i,j) is referred to as a pixel. Let $\mu(i,j)$ denote the mean of X(i,j). $\epsilon(i,j) = X(i,j) - \mu(i,j)$ is referred to as noise. $\epsilon(i,j)$ is called Gaussian noise if X(i,j) is Gaussian distributed, and Poisson (or Poisson-type) noise if X(i,j) is Poisson distributed. The following theorem states the distribution of the wavelet phase of Gaussian noise under the 2D symmetric Haar transform.

**Theorem 1:** Suppose that {$\epsilon$(i,j): (i,j)$\in$ **L**} are independent Gaussian noises (both with mean zero, though possibly with different variances). Let $W_x\epsilon(i,j)$ and $W_y\epsilon(i,j)$ denote the components of the 2D symmetric Haar transform of $\epsilon(i,j)$. Then $\theta(i,j) = \text{Arctan}\frac{W_y\epsilon(i,j)}{W_x\epsilon(i,j)}$ is uniformly distributed on $[0, 2\pi)$ for each (i,j).

For each pixel (i,j), let $\epsilon_n(i,j)$ be a sequence of Poisson noise with variance $n\mu(i,j)$. The Poisson noise $\epsilon_n(i,j)$ is said to be regular if for disjoint $(i_1,j_1)$ and $(i_2,j_2)$, (i) $\epsilon_n(i_1,j_1)$ and $\epsilon_n(i_2,j_2)$ are independent; (ii) $\frac{\epsilon_n(i_1,j_1)}{\sqrt{n\mu(i_1,j_1)}}$ and $\frac{\epsilon_n(i_2,j_2)}{\sqrt{n\mu(i_2,j_2)}}$ converge in distribution to two independent standard Gaussian random variables as $n \to \infty$. For the 2D wavelet transforms of the regular Poisson noise, we have the following main theorem:

**Theorem 2:** Let $W_x\epsilon_n(i,j)$ and $W_y\epsilon_n(i,j)$ denote the components of the 2D symmetric Haar transform of regular Poisson noise $\epsilon_n(i,j)$. Then $\text{Arctan}\frac{W_y\epsilon_n(i,j)}{W_x\epsilon_n(i,j)}$ converges in distribution to a random variable which is uniformly distributed on $[0, 2\pi)$ as $n \to \infty$.

The significance of Theorem 1 is that even though the variance of the noise can change from pixel to pixel, the phase of the Haar type wavelet transform is identically distributed at each location. Furthermore, the phases at nearest neighbor locations are uncorrelated in the wavelet transform at scale 1. (Correlation in other neighboring locations introduced by the wavelet transform, if any, is a problem to be further investigated, but such spurious correlation seems not to affect our numerical results.) The significance of Theorem 2 is that as $n$ increases, that is to say, as the time of observation for the emission tomography image increases, the Poisson type noise becomes more and more similar to the Gaussian noise needed to apply Theorem 1. Theorem 2 is essentially a central limit theorem result.

**Wavelet Phase Based Denoising Schemes.** Based on the wavelet phase properties explored above, we developed the following denoising algorithms:

*I. Edge Tracking.* As shown above, the wavelet phase of regular Poisson noise is asymptotically uniformly distributed on $[0, 2\pi)$. On the other hand, the "true edges" of an image separate two neighboring regions and the neighboring edge pixel usually have similar gradient directions. Since the phase of wavelet transform of an image is the gradient direction of a smoothed version of the image, it is reasonable to say that, for a true edge, there must exist at least one neighboring edge pixel in a direction roughly orthogonal to the gradient direction, which has roughly similar wavelet phase. Otherwise, the edge pixel is most likely caused by noise. We developed a numerical algorithm called "edge tracking" scheme to implement this idea. For details of the scheme, we refer the reader to [LIN94].

*II. Local Phase Variance Thresholding.* Another denoising scheme of exploiting wavelet phase is to consider local wavelet phase variation. For each scale k and each pixel (i,j), let

$$\overline{W}_x^k f(i,j) = \sum_{m=-M_k}^{M_k} \sum_{n=-M_k}^{M_k} W_x^k f(i+m, j+n)$$

and

$$\overline{W}_y^k f(i,j) = \sum_{m=-M_k}^{M_k} \sum_{n=-M_k}^{M_k} W_y^k f(i+m, j+n)$$

where $M_k$ is a positive integer. The mean wavelet phase at (i,j) is defined by

$$\overline{P}^k f(i,j) = \text{Arctan} \frac{\overline{W}_y^k f(i,j)}{\overline{W}_x^k f(i,j)}.$$

The difference between the phase of $(W_x^k f(i,j), W_y^k f(i,j))$

$$P^k f(i,j) = \text{Arctan} \frac{W_y^k f(i,j)}{W_x^k f(i,j)}$$

and $\overline{P}^k f(i,j)$ is expected to be small if the pixel (i,j) is "true edge" but large if the pixel (i,j) is an edge generated by noise. Therefore, one might distinguish true edges from noisy edges by thresholding $P^k f(i,j) - \overline{P}^k f(i,j)$. This technique is called "local phase variance thresholding".

*III. Scale Phase Variation Thresholding.* We can also discriminate noisy edges from true edges by considering phase changes from scale to scale. For a true edge, the wavelet phase should not change very much from scale to scale, since the image at each scale is a smoothed version of the image of the previous scale. But for a spurious edge due to noise, the independence of the noise at different locations can be expected to lead to different wavelet phases at different scales. This observation leads to a denoising technique we call "scale phase variation thresholding": if $|P^{k+1}(i,j) - P^k(i,j)|$ exceeds a threshold, the edge pixel is discarded as spurious at both scales $k$ and $k+1$.

# 3 Numerical Experiments

We conducted numerical experiments in a SUN workstation with Xwindow system. The programs are written in C and FORTRAN languages; some IMSL (International Mathematics and Statistics Library) routines were called to generate Poisson random numbers. Figure 1 is the Shepp-Logan phantom. It consists of 10 ellipses, each with a different gray level. This phantom has been used as a standard to test the accuracy of restoration algorithms. Figure 2 is the "ray-sum image" (or undistorted sinogram) of the Shepp-Logan phantom. A simulated sinogram is given in Figure 3. Figures 4 to 8 give some numerical results obtained in this study. The size of the original image (Shepp-Logan phantom) is $128 \times 128$ and the size of the sinogram is $180 \times 128$, though in Figures 2 and 3, we display only the first 128 rows of the sinogram. The pixel values of all images are normalized to 8 bits (ranged from 0 to 255). The same noisy sinogram, shown in Figure 3, was used for all of Figures 4 through 8; it had a total of about 2 million photons.

Figure 4 is the image reconstructed from noisy sinogram using convolution back projection (CBP) method. Small features in the Shepp-Logan phantom are virtually undetectable. This indicates that a filtering algorithm is necessary before applying the CBP algorithm. Figure 5 is the image reconstructed from the noisy sinogram, using CBP in conjunction with a parabola filter. Some small features present in the Shepp-Logan phantom can be discerned, but the image is blurred. Figure 6 is the image reconstructed from the noisy sinogram, using CBP with a wavelet modulus filter. To obtain Figure 6, a wavelet transform was performed up to 3 scales. Modulus thresholding values were 0.2 for scale 1, 0.1 for scale 2 and 0.05 for scale 3. The decay rate from one scale to the next was thresholded by 0.1. (These values were determined by trial and error and are roughly optimal among the values considered.) Some small features of the Shepp-Logan phantom can be discerned in Figure 6, but the image quality is not good, perhaps inferior to that of Figure 5. Figures 7 and 8 are images obtained from the noisy sinogram using CBP combined with one of the wavelet phase filters proposed here. In Figure 7, the wavelet phase filter is used with a wavelet modulus filter of the sort used in obtaining Figure 6; Figure 8 was obtained without any wavelet modulus filter. The phase variation from one scale to the next is thresholded to be $\frac{\pi}{6}$. In Figures 7 and 8, two small features of the Shepp-Logan phantom can be seen fairly clearly, though others, notably those at the bottom of the phantom near the center, are still not so clear.

On the basis of subjective evaluation of the restored PET images, it appears to us that features of the original image are restored somewhat more clearly using the wavelet phase filter than using the wavelet modulus filter, compare Figure 7 or Figure 8 with Figure 6, and also that the wavelet phase filter outperforms the conventional linear low pass filter, compare Figure 7 or Figure 8 with Figure 5. Further evaluation of results is a matter for future research. We claim that the evidence suggests, at the very least, that the wavelet phase filter shows promise for emission tomography imaging.

## REFERENCES


[KUAN85] D. T. Kuan, A. A. Sawchuk, T. C. Strand and P. Chavel, "Adaptive noise smoothing filter for images with signal-dependent noise", *IEEE Trans. Patt. Anal. Machine Intell.*, Vol. PAMI-7, No. 2, pp. 165-177, Mar. 1985.

[LIN94] B. Lin, "Wavelet Phase Filter for Denoising in Tomographic Image Reconstruction", Ph.D. Thesis, Illinois Institute of Technology, Dec. 1994.

[LEWI86] R. M. Lewitt and G. Muehllehner, "Accelerated iterative reconstruction for positron emission tomography based on the EM algorithm for maximum likelihood estimation", *IEEE Trans. Med. Imaging*, Vol. MI-5, No. 1, pp. 16-22, Mar. 1986

[MALL92a] S. Mallat and S. Zhong, "Characterization of signals from multiscale edges", *IEEE Trans. Patt. Anal. Machine Intell.*, Vol. 14, No. 7, pp. 710-732, July 1992.

[MALL92b] S. Mallat and W. L. Hwang, "Singularity detection and processing with wavelets", *IEEE trans. Inform. Theory*, Vol. 38. No. 2, pp. 617-645, Mar. 1992.

[MARR80] D. Marr and E. Hildreth, "Theory of edge detection", *Proc. Roy. Sco. Lon.*, Vol. 207, pp. 187-217, 1980.

[SHEP82] L. A. Shepp and Y. Vardi, "Maximum likelihood reconstruction in positron emission tomography", *IEEE Trans. Med. Imaging*, Vol. MI-1, No. 2, pp. 113-122, Oct. 1982

[STAR81] H. Stark. J. Wood, I. Paul and R. Hinorsni, "Direct Fourier reconstruction in computer tomography", *IEEE Trans. Acoust. Speech Signal Proc.*, Vol. ASSP-29, pp. 237-245, April 1981.

[VARD85] Y. Vardi, L. A. Shepp and L. Kaufman, "A statistical model for positron emission tomography", *J. Amer. Statist. Assoc.*, Vol. 80, pp. 8-20, Mar. 1985.

[YANG91] D. Yang, "Noise smoothing in direct Fourier positron emission tomography", M.S. thesis, Illinois Institute of Technology, Dec. 1991.

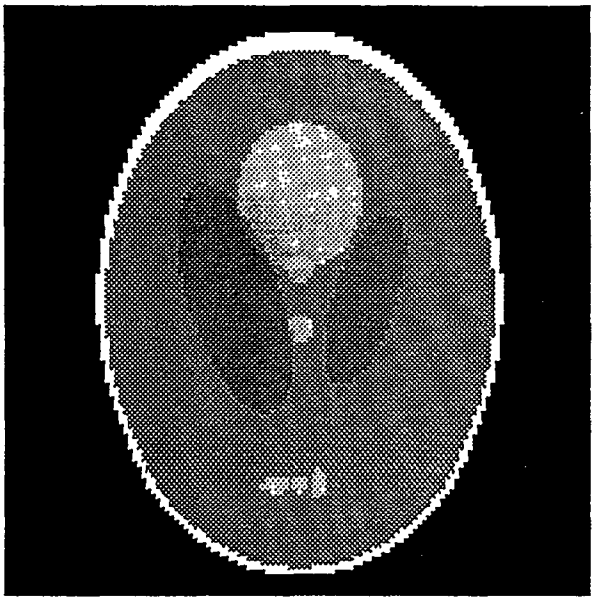

Fig. 1. Shepp-Logan Phantom

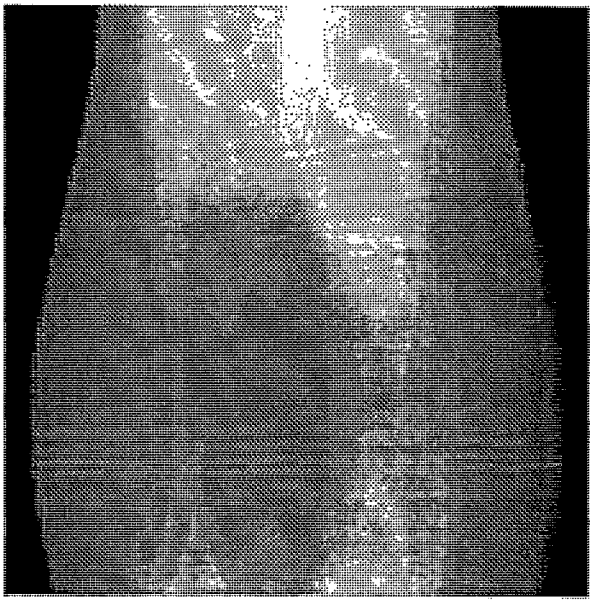

Fig. 2. Raysum Image

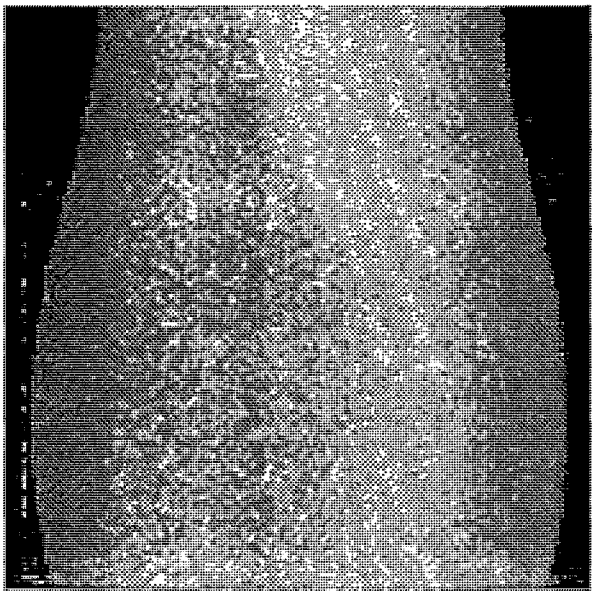

Fig. 3. Noisy Raysum

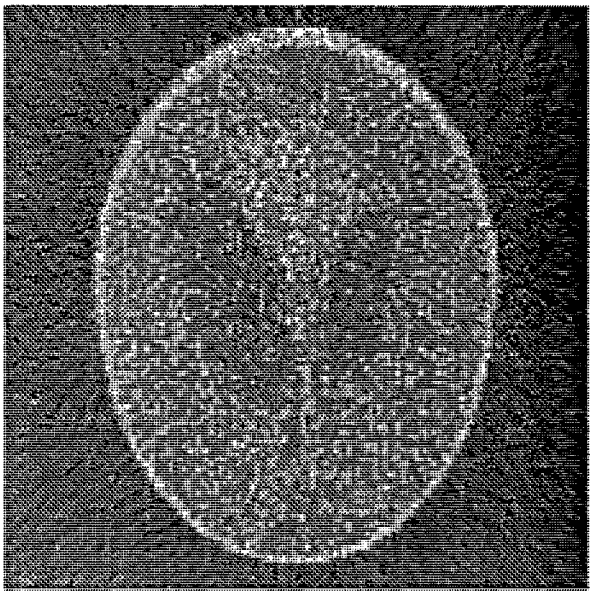

Fig. 4. CBP Reconstruction

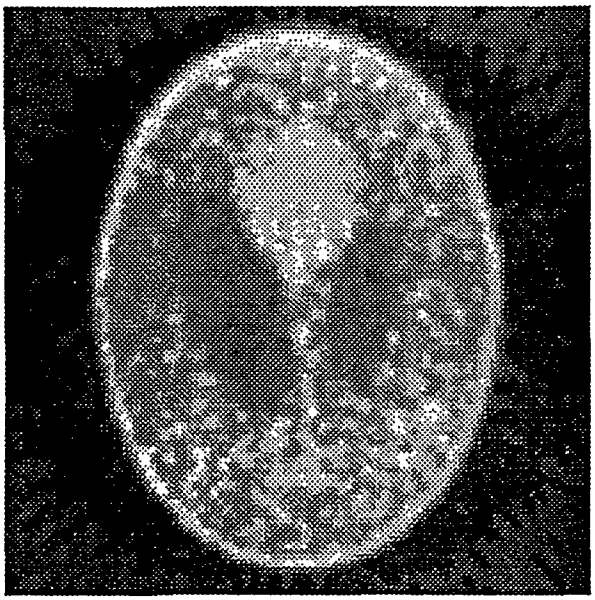

Fig. 5. Parabola Filter

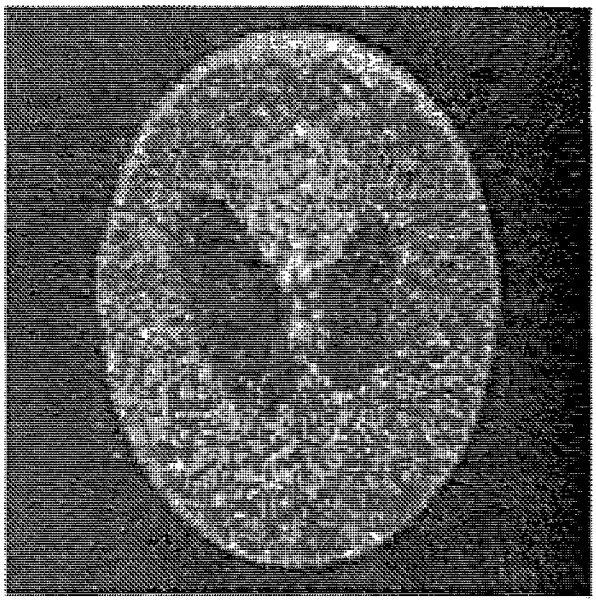

Fig. 6. Wavelet Modulus Filter

Fig. 7. Modulus+Phase Filter

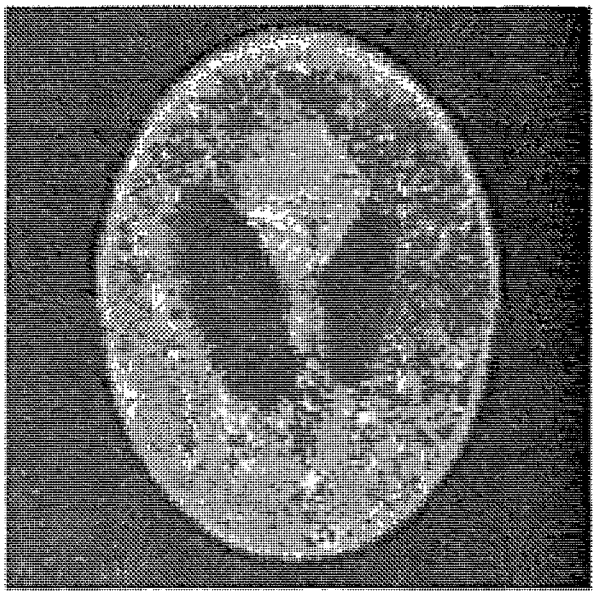

Fig. 8. Wavelet Phase Filter